Thermal Transport in Graphene Nanostructures: Experiments and Simulations

Luis A. Jauregui[a,b], Yanan Yue[c], Anton N. Sidorov[d], Jiuning Hu[a,b], Qingkai Yu[e], Gabriel Lopez[a,b], Romaneh Jalilian[a,f], Daniel K. Benjamin[d], Derek A. Delk[d], Wei Wu[e], Zhihong Liu[e], Xinwei Wang[c], Zhigang Jiang[d], Xiulin Ruan[g], Jiming Bao[e], Steven S. Pei[e], Yong P. Chen[a,b,f]

[a] Birck Nanotechnology Center, Purdue University, West Lafayette, IN 47907
[b] School of Electrical and Computer Engineering, Purdue University, West Lafayette, IN 47907
[c] Department of Mechanical Engineering, Iowa State University, Ames, IA 50011
[d] School of Physics, Georgia Institute of Technology, Atlanta, GA 30332
[e] Department of Electrical and Computer Engineering, University of Houston, Houston, Texas 77204
[f] Department of Physics, Purdue University, West Lafayette, IN 47907
[g] School of Mechanical Engineering, Purdue University, West Lafayette, IN 47907

Thermal transport in graphene and graphene nanostructures have been studied experimentally and theoretically. Methods and previous work to measure and calculate the thermal conductivities of graphene and related nanostructures are briefly reviewed. We demonstrate that combining Raman spectroscopy for thermometry and electrical transport for Joule heating is an effective approach to measure both graphene thermal conductivity and graphene-substrate interface thermal resistance. This technique has been applied to a variety of exfoliated or CVD-grown graphene samples (both suspended and substrate-supported), yielding values comparable with those measured using all-optical or all-electrical techniques. We have also employed classical molecular dynamics simulation to study thermal transport in graphene nanostructures and suggest such structures may be used as promising building blocks for nanoscale thermal engineering.

Introduction

Graphene is a recently discovered material (1) with highly promising electronic properties. The thermal properties of graphene are also impressive. Graphene presents some of the highest values for thermal conductivity at room temperature (~3000-5000 W/m-K (2, 3) among known materials. This extremely high thermal conductivity opens up a variety of applications, such as thermal management. In this work, we have measured the thermal conductivity of graphene and the interface thermal resistance between graphene and the substrate (SiO_2/Si). Our primary experimental approach is a combination of Raman spectroscopy and electrical current heating, where Raman spectrum is used as a thermometer. The measurement is done at room temperature. We also present a simple, low-cost all-electrical method to estimate the thermal conductivity of large size graphene films (such as those grown by chemical vapor deposition). Our measurements confirm the excellent thermal conductivity of graphene and graphene-substrate interface thermal resistance previously measured with different techniques or with different graphene materials.

The possibility of nanoscale thermal devices to control nanoscale heat flow has gained considerable interests recently (4-6). We have also employed classical molecular dynamics simulation to study thermal transport in graphene nanostructures and suggest such structures may be used as promising building blocks for nanoscale thermal engineering.

Experimental Measurements

Three main methods to measure the thermal conductivity and the thermal interface resistance of graphene have been previously used: purely optical (2, 3), electrical burning (7) and electrical 3-omega method (8). For the optical method, shift in the Raman spectra peak was used to monitor the temperature while changing the power of the Raman laser (2, 3). Temperature dependence of Raman G peak position for single and bilayer graphene has calibrated as -0.015 and -0.016 cm^{-1}/K for bi and single layer suspended graphene respectively (9, 10). As temperature increases, the G peak position undergoes a red shift, explained theoretically by a four-phonon interaction dominating the decrease in the bond length with increasing temperature (11). Red shifts in peak positions of G and 2-D peaks of spatially resolved Raman spectra were used to measure the temperature distribution in biased supported graphene transistors (12), where peak operating temperatures of 1000K where found in the middle of the graphene. The electrical burning method studied parallel supported graphene nanoribbons, and the current is ramped until the graphene ribbon reaches the breakdown current and burn (7). The 3-omega method was used to measure the thermal contact resistance of single and few layers graphene flakes on SiO_2 (on Si) and no significant difference is found for different thickness, and the value measured is lower than carbon nanotubes (8). Due to the high value of thermal conductivity measured on graphene, it has great promise in potential applications in thermal management such as heat dissipation (13).

Raman spectra as thermometry for graphene. Both the frequency and amplitude of Raman spectrum of graphene can depend on temperature and be used as intrinsic, material (graphene) specific thermometers. Each choice has its own advantages. For example, Raman peak frequency and its temperature dependence are generally more universal for different graphene samples and used in previous works (2, 3). The Raman peak amplitude and its temperature dependence can vary considerably for different samples and measurements, but the amplitude can also show more sensitive change with temperature.

Graphene Sample Preparation

Two types of graphene have been studied in our work: 1) Graphene mechanically exfoliated from highly ordered pyrolytic graphite (HOPG), using scotch tapes (1). Graphene is commonly transferred to a highly doped silicon wafer with 300nm thermally grown SiO_2. Afterwards, an optical microscope is used to find graphene by optical contrast (14); 2) Graphene grown by chemical vapor deposition (CVD) on polycrystalline Ni (15) or Cu (16) foils. The precursor gas used is methane. To transfer graphene to other substrates, samples are coated by PMMA, and then metal (Ni or Cu) is etched. Then graphene/PMMA films are scooped out from the solution and rinsed with DI water, and placed onto the substrate (eg. SiO_2/Si). This paper will focus on data measured in CVD graphene, whose thermal transport has not been addressed previously.

In order to suspend CVD graphene to accurately measure its thermal conductivity (reducing the heat leakage via substrate), we deposit 35 nm of Cr and 50 nm of Au by thermal evaporation onto a 300nm thick SiO_2 thermally grown on highly doped Si wafer. Then, 10μm-width trenches are defined onto a $1cm^2$ chip by e-Beam lithography and wet etching. A 3mm width and 6mm long CVD graphene coated by PMMA samples is deposited onto the predesigned electrode-trenches. PMMA is later removed by acetone and a subsequent critical point drying process is used in order not to break the suspended graphene by surface tension.

Measurement of graphene-substrate interface thermal resistance

In this technique, a Raman microscope with the probing laser of 532 nm excitation wavelength was used to detect the Raman signal. The graphene sample (supported on SiO_2/Si) with an area (A) of 1.26×10^{-8} m^2 (shown in Fig. 1a is a few-layer CVD-grown graphene sample) and electrical resistance (R) of 134 Ω was placed in a fully-closed chamber for Raman spectroscopy experiment. In the calibration experiment, the sample was heated by a flexible heater up to 120 ^oC, and a T type thermocouple was attached on the sample surface to measure the temperature in real-time. Several Raman spectra were captured at different constant temperatures, as shown in Figure 1b. After the normalization with respect to the Raman peak height at room temperature, relationships between temperature and relative peak intensities of silicon, G band and D´ band of graphene were established respectively, as shown in Figure 1c. The calibration establishes the Raman peak intensity as a thermometer for this sample.

In the interface thermal resistance measurement, the ends of sample were glued by the silver paste to the outstretched electrical wires which were connected to a high-precision DC power supply. The electrical joule heating will induce a temperature rise in the sample and the heat will go though the SiO_2 to the silicon substrate. Then, combing with the established calibration results, the temperatures of graphene and silicon can be monitored by the corresponding Raman signals. The interface thermal resistance $r=\Delta T/(I^2R/A)$, where I^2R/A is electrical heating power density and ΔT is the temperature difference between graphene and substrate. The total thermal resistance r from graphene film to the upper surface of silicon substrate can be calculated by the difference of the temperature-power density slope for the two materials (Fig. 1d). In this experiment, a DC power supply was used to provide the DC current from 0 to 30mA. From Figure 1d, the total thermal resistance is calculated as 3.13×10^{-7} $K\cdot m^2/W$.

The total thermal resistance includes three components: thermal resistance of silicon (r_{Si}), thermal resistance of SiO_2 (r_{SiO2}) and the thermal contact resistance at the graphene-SiO_2 interface (r_{tc}). The absorption depth (τ) of Si is calculated as 1.28×10^{-6} m at 532 nm. And r_{Si} can be computed by $\tau/(2k_s)$ as 4.33×10^{-9} $K\cdot m^2/W$, where k_s is thermal conductivity of Si (150 W/m·K). r_{SiO2} is calculated by L/k as 2.14×10^{-7} $K\cdot m^2/W$, where L is the thickness (300 nm) of SiO_2 and k is its thermal conductivity (1.4 W/m·K). Therefore, the thermal contact resistance at the graphene-SiO_2 interface is 9.5×10^{-8} $K\cdot m^2/W$. Comparison of our result with other published results is summarized in Table II at the end of this paper.

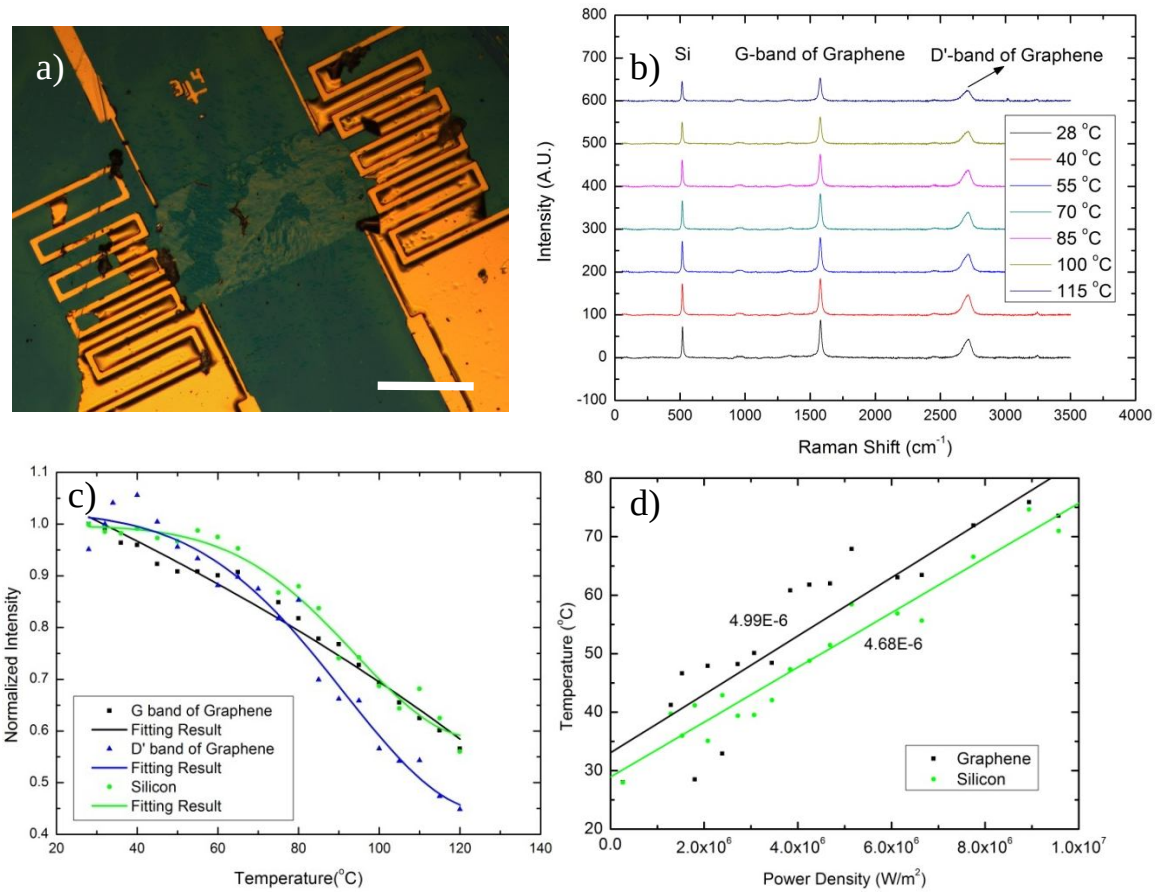

Figure 1 (a) Photo of the CVD few-layer graphene sample. (b) Raman spectra at different temperatures in the calibration. (c) The correlation between the temperature and normalized Raman peak heights (for silicon and the graphene G and D' bands). (d) The relationship between power density (joule heating) and temperature of graphene and silicon. The solid lines are the best linear fitting results, and the slopes are 4.99×10^{-6} and 4.68×10^{-6} for graphene and silicon, respectively.

Measurement of graphene thermal conductivity

To measure the thermal conductivity of graphene, we used suspended CVD graphene devices to remove the heat leakage from substrate. The suspended graphene device is wirebonded to a commercial chip carrier (CERQUAD). The chip is electrically connected to a variable temperature microscope stage-vacuum chamber (Instec HCS622V) to perform electrical and Raman measurements. A Raman microscope is used with a 532nm laser. A 100X large-working distance lens is used as the objective. DC currents are passed through graphene. The graphene resistance for most of our samples is independently measured by 4-probe measurements. The current used range from 0mA to 30mA and Raman spectra are taken from the middle of the sample for different currents, as shown in Fig. 2b for a sample "1" (trench length= 20μm and graphene width~13mm). The D' (2-D) Raman peak obtained from sample 1 show a reduction of amplitude of ~50% at 30mA. Using the typical calibration as shown in fig. 1c, the temperature rise in the sample center is ~100K.

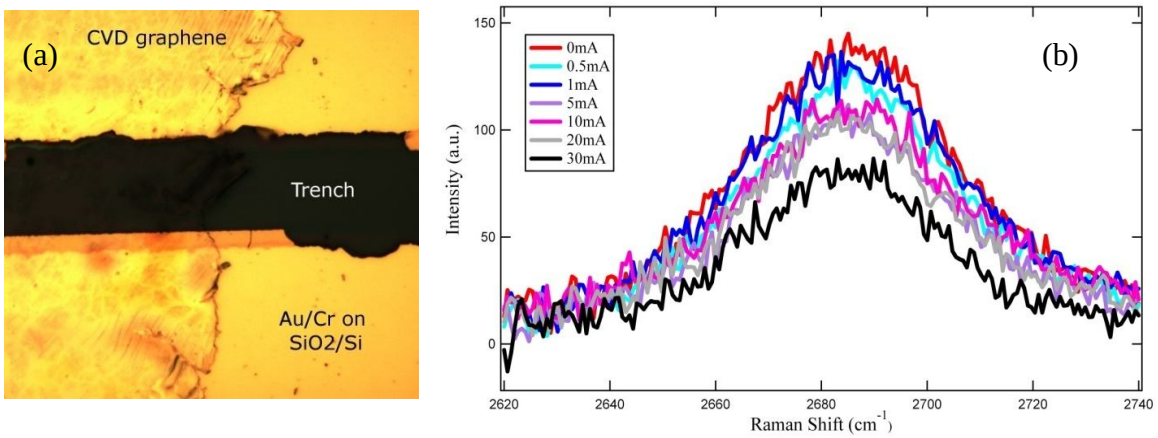

Figure 2. a) 100X magnified optical image of a suspended CVD graphene on Au/Cr/SiO_2 trench, b) Raman 2D-peak from the middle of the suspended graphene sample "1".

The thermal conductivity of the suspended graphene can be extracted with a simple model to a good approximation. For a suspended rectangular-shaped graphene, the majority of the Joule heat generated by applying electrical current I is dissipated in the plane of the graphene. We assume that the heat dissipation out of the plane of GNR is negligible and the temperature profile transverse to the electrical current and the Joule heating rate are both uniform. The 3-dimensional heat transfer equation in GNR is thus reduced to a 1-dimensional equation:

$$\kappa d^2T/dx^2 + RI^2/(LWh) = 0 \qquad [1]$$

where κ is the thermal conductivity of graphene, T(x) is the temperature profile along the direction of the current, R is the resistance of the graphene, L is the length of the suspended graphene along the direction of the current, W is the width and h (=0.335 nm) is the thickness. Suppose the temperature at $x=\pm L/2$ is the same as the temperature T_0 of contacts, then the temperature profile is

$$T(x) = T_0+RI^2(L^2/4-x^2)/(2LWh\kappa). \qquad [2]$$

The maximum temperature $T_m= T_0+RI^2L/(8Wh\kappa)$ appears at x=0 (center).

The thermal conductivity can be extracted as:

$$\kappa = RI^2L/ (8\Delta TWh), \qquad [3]$$

where $\Delta T=T_m-T_0$ is the difference between the maximum temperature at the center and the contact temperature (~300K in our case).

Using equation [3] and R~1 kOhm, I = 30mA, L = 20um, ΔT~100K, W ~ 1.3cm and h = 0.35nm, we obtain κ at room temperature is ~5000 W/m-K. We note the finite-size laser spot on the graphene may be slightly off the center and underestimate the actual T_m and overestimate κ. We have also used the temperature induced shift of Raman G-peak frequency calibrated by Calizo *et al* (9, 10) as another thermometer and measured a number of suspended CVD and exfoliated graphene samples and obtained thermal conductivity ranging from ~1500 – 4000 W/m-K. The details of these measurements will

be presented elsewhere. Comparison of our result with other published results is summarized in Table I at the end of this paper.

All-electrical measurement. For macroscopic-size CVD graphene, we demonstrate that an estimate of graphene thermal conductivity (at room temperature) can be made using a relatively straight forward all-electrical method using standard thermal couples, even for graphene supported on substrates. In this case, we use a miniature heater and two differential thermocouples, as shown in the Figure 3 (a) and (b) below. The heat generated by the heater creates a temperature gradient across the graphene and the Au pads deposited at both ends. The substrate is made of glass, a poor thermal conductor at room temperature. The two identical differential thermocouples are placed across the graphene and on the Au pad away from the heater, respectively. Each differential thermocouple consists of two Cr-Al (chromel-alumel) junctions and measures the temperature differential (ΔT) between them. The thermocouple voltage vs. temperature calibration is provided by NIST ITS-90 Thermocouple Database, and $\Delta V \propto \Delta T$ for the temperature range of our measurements.

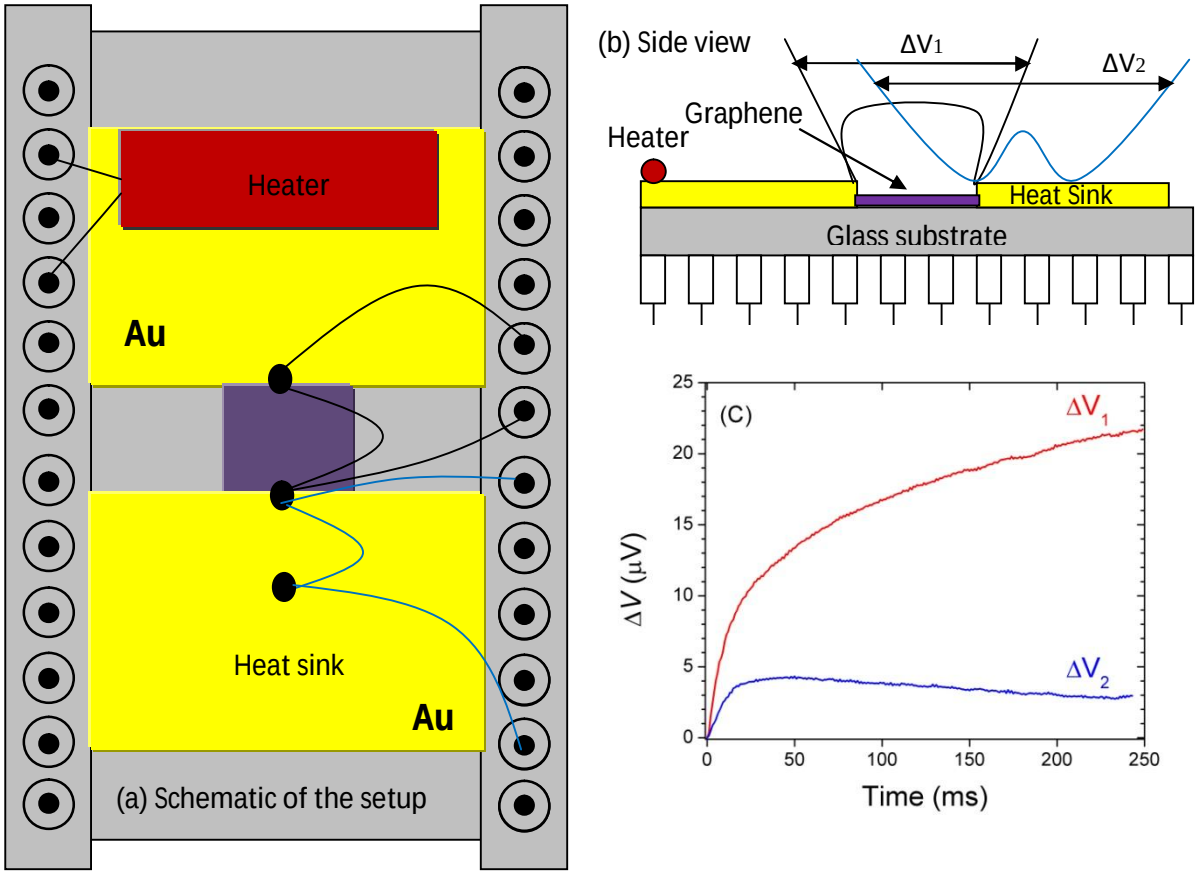

Figure 3. (a) Schematic of the all-electrical thermal conductivity measurement for large-size CVD graphene. (b) Side view of the experimental setup. (c) Response of the two differential thermocouples after turning on the heater.

Conceptually, thermal conductivity (κ) is defined as the quantity of heat (Q) transmitted per unit length (ΔL) and per unit cross section area (A) due to a unit temperature gradient, i.e., $\kappa = Q \times \frac{\Delta L}{\Delta T \times A}$. If one assumes the heat transmitted through graphene is approximately equal to that through the Au pad, the thermal conductivity of graphene $\kappa_g = \kappa_{Au}\left(\frac{\Delta T_2}{\Delta T_1}\right)\left(\frac{A_2}{A_1}\right)\left(\frac{\Delta L_1}{\Delta L_2}\right) \approx 7000$ $Wm^{-1}K^{-1}$ (subscript 1 indicates graphene, subscript 2 indicates Au) where $\kappa_{Au} = 318$ $Wm^{-1}K^{-1}$ (based on Goodfellow.com technical reference), $\frac{A_2}{A_1} = 274$ and $\frac{\Delta L_1}{\Delta L_2} = 0.590$ from dimension measurements, and $\frac{\Delta T_2}{\Delta T_1} = \frac{\Delta V_2}{\Delta V_1} = 0.136$ as indicated in Figure 3 (c).Two major sources of uncertainty in the above crude estimate are: 1) The measured ΔV_1 is not yet saturated in Fig 3 (c), which would *overestimate* κ_g; 2) The heat leak through the glass substrate means the heat transmitted in the Au pad (away from the heater) is actually less than that in graphene. This would *underestimate* κ_g. Nonetheless, this simple, low-cost technique (lithography-free and using off-the-shelf components) can give a quick estimate for κ_g that is on the same order of magnitude as measured by other methods.

Molecular Dynamics Modeling

Review of the theory of thermal transport in graphene

Graphene has many unique thermal transport properties. Many theoretical models have been proposed and applied to explain and predict the thermal properties of graphene.
Classical molecular dynamics (MD) is widely used in calculating the thermal conductivities of graphene nanoribbons (GNRs), because the electronic contribution to the thermal conduction in graphene can be neglected compared to the contribution from the lattice part (3) at room temperature. For a GNR of about 6 nm×1.5 nm, its thermal conductivity is calculated to be ~2000 W/m-K (17), comparable with the experimental values, but it is argued that the corresponding thermal conductance is far beyond the ballistic limit (18). Due to the limited calculation capacity of MD, it is impractical to simulate macro-scale (bulk) graphene. Nevertheless, it is shown (19) that the thermal conductivity exponentially depends on the length of GNRs up to 60 nm long, suggesting that graphene has very long phonon mean free path. When applied compressive/tensile strain along the temperature gradient of GNRs, their thermal conductivity is remarkably reduced (19). Like the electronic transport in carbon nanotubes, the thermal transport in GNRs also depends on the edge chirality. The MD simulation has showed that the GNRs with zigzag edges along the temperature gradient have larger thermal conductivity than that with armchair edges (17). Qualitatively consistent results have been obtained by others (18, 20) using ballistic phonon transport equations. The crystal directional dependence of the thermal conductivity will become negligibly weak for intrinsic graphene, i.e., the thermal conduction in graphene should be isotropic. The difference between the thermal transport of GNRs and intrinsic graphene opens the possibility to control heat transport in GNRs related devices. MD is also applied to study the isotope effect on the thermal conductivity of GNRs (21). The thermal conductivity is reduced after mixing different carbon isotopes, and the reduction is strongly related to the pattern of the mixing. It is found that GNRs composed of alternative C^{12} and $C^{13/14}$ slices can

induce much more reduction of the thermal conductivity than the case of random mixing. Similar results have been obtained from the nonequilibrium Green's function (NEGF) method for zigzag GNRs. A first-principle calculation also confirms that the reduction of the thermal conductivity is due to the phonon scattering by the isotope clusters (22). Another interesting observation from MD, the thermal rectification (17), is found in asymmetrical GNRs. In the asymmetrical triangular GNRs, the thermal conductivity from the wider end to the narrower end can be twice larger than that from the narrower to the wider end at temperature of ~ 200 K. Thermal rectifications is also confirmed in T-shaped asymmetric GNRs (23). Kong et al. (24) used density functional theory to compute the phonon spectrum and life time and then calculated the temperature dependent thermal conductivity. The calculated result is about 2200 W/m-K at 300 K. It is also shown that the thermal conductivity has the power law dependence of temperature of T^{-1} at high temperature. Similarly, by calculating the Gruneisen parameters of graphene from first principles (25), it is shown that the thermal conductivity is in the range of 2000-5000 W/m-K for monolayer graphene flakes with different width, defect concentration and edge roughness.

Molecular Dynamics (MD) Simulation

The Brenner potential (26), successfully applied to many hydrocarbon systems, is employed in the classical MD simulation. To drive a heat current in GNRs, we place the atoms at two ends of GNRs in two Nosé-Hoover (27, 28) thermostats at different temperatures. The thermal conductivity (κ) can be calculated from the Fourier's law $\kappa=Jd/(\Delta Twh)$ where J is the heat current, ΔT is the temperature difference of the two thermostats, d is the length, w is the width and h is thickness of GNRs. The equations of motion for atoms in the thermostat with desired temperature T_0 are:

$$d\mathbf{p}_i/dt=\mathbf{F}_i-\gamma\mathbf{p}_i,\ d\gamma/dt=[T(t)-T_0]/(\tau^2T_0),\ T(t)=\Sigma_i\mathbf{p}_i^2/(3mNk_B) \qquad [4]$$

where i runs over all atoms in the thermostat, $\mathbf{p}_i$ is the momentum of the i-th atom, $\mathbf{F}_i$ is the total force applied on the i-th atom, γ is the dynamical parameter with zero initial value, τ is the relaxation time, m is the mass of carbon atoms, N is the number of atoms in the thermostat and k_B is the Boltzmann constant. The j-th atom not in any thermostat is just described by the Newton's law $d\mathbf{p}_j/dt=\mathbf{F}_j$. More numerical details about the simulation can be found in Ref. (17). As an example, the temperature dependent thermal conductivity of an armchair GNR is shown in Fig. 4 (a).

MD simulation can be used to study diverse thermal transport phenomena in graphene nanostructures and to design interesting nanoscale thermal devices. We present here a few illustrative examples. We calculated specific heat capacity (c_p) and thermal diffusivity ($\kappa/\rho c_p$, where is mass density) of the above GNR as a function of T in the range 100-300 K. The results are shown in Figure 4(b). We also studied a 3-terminal device shown in the inset of Fig. 7, the temperature at the "source" and "drain" are kept at constant T_S=100 K and T_D=300 K. By varying the temperature T_G at the "gate" from 60 K to 340 K, the heat current flow into the device from drain is not a monotonic function of the temperature difference T_{DG} between drain and gate, as shown in Fig. 5. For T_{DG} in the range of 160-220 K, the heat current decreases as T_{DG} increases, which indicates negative differential thermal conductance and it may be useful in nonlinear control of heat transport, and design of "thermal logic" or "thermal transistors" (6,29).

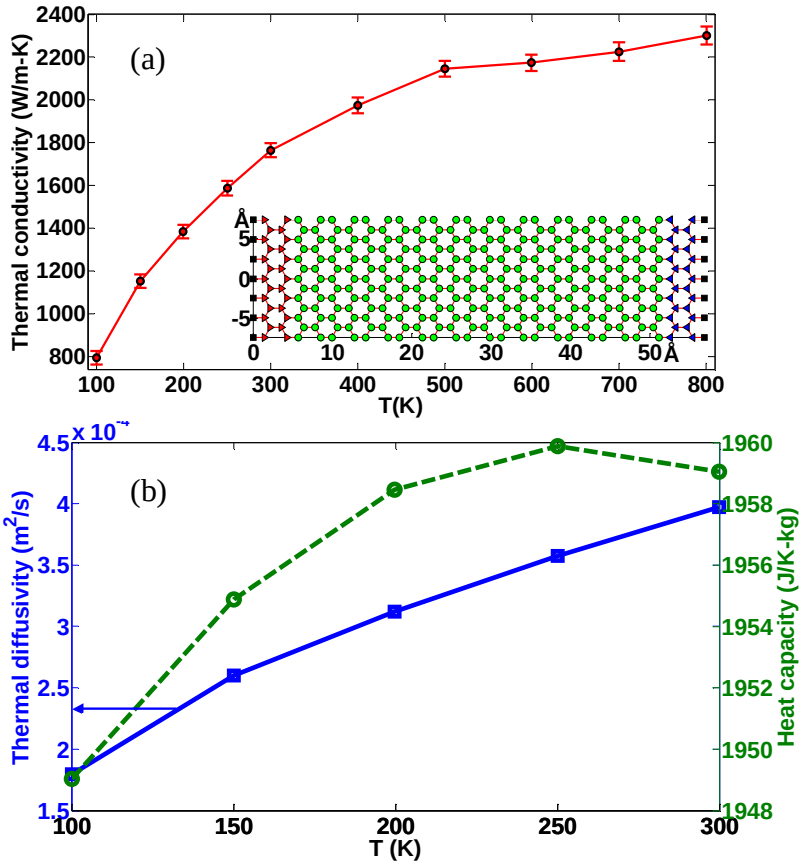

Figure 4. (a) Temperature dependent thermal conductivity of an armchair GNR shown in the inset. The position of atoms denoted by squares is fixed. The atoms denoted by right- and left-pointing triangles are placed in two different thermostats. The remaining atoms denoted by circles are not in any thermostat. (b) Thermal diffusivity (left axis with solid line) and heat capacity (right axis with dashed line) as a function of temperature.

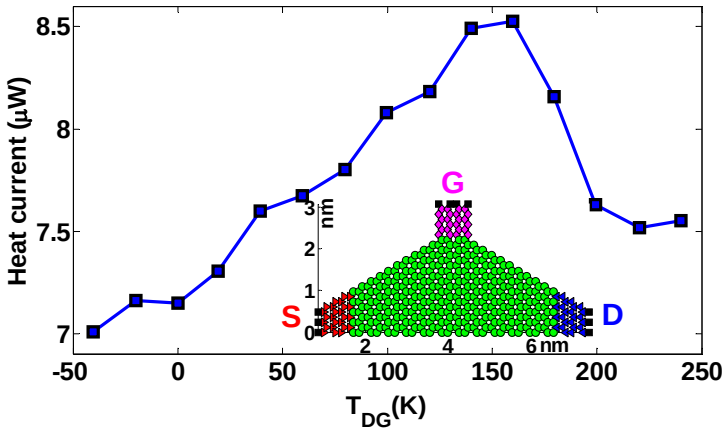

Figure 5. The heat current in drain vs. the temperature difference T_{DG} between drain and gate in a 3-terminal device. The inset shows the structure of the 3-terminal device. The atoms in source (S), drain (D) and gate (G) are denoted by right-pointing triangles, left-pointing triangles and diamonds respectively.

Summary

We have studied thermal transport in various graphene nanostructures experimentally and by MD simulation. Our results and those from other published works are summarized in the 3 tables in the following:

TABLE I. Measured thermal conductivity (κ) of graphene (300K).

κ (W/m-K)	**Methods**	**Material type**	**Ref.**
3080 – 5150	Raman	Suspended exfoliated graphene	(3)
4840 – 5300	Raman	Suspended exfoliated graphene	(2)
1100	Electrical burning	Substrate-supported exfoliated graphene nanoribbons	(7)
1500 – 5000	Raman+Electrical	Suspended CVD graphene	This work
~7000 (crude estimate)	All electrical	Substrate-supported CVD graphene	This work

TABLE II. Measured thermal interface resistance (r) between graphene and SiO_2/Si (300K).

r (Km^2/W)	**Methods**	**Material type**	**Ref.**
$4x10^{-8}$	Raman + Electrical	Substrate-supported exfoliated graphene	(12)
$5.6x10^{-9} – 1.2x10^{-8}$	3-omega	Substrate-supported exfoliated graphene	(8)
$9.5x10^{-8}$	Raman + Electrical	Substrate-supported CVD-grown graphene	This work

TABLE III. Calculated thermal conductivity (κ) of graphene (300K).

κ (W/m-K)	**Methods**	**Material type**	**Ref.**
~2000	Classical MD	~1.5 nm×6 nm GNRs	(17)
~ 200-800	Classical MD	~2 nm×11-60 nm GNRs	(19)
~2200	First principle	Bulk graphene	(24)
~2000-5000	First principle and phonon Boltzmann equation	Bulk graphene	(25)

Acknowledgments

We acknowledge Miller Family Endowment, Birck Director's Fund, Semiconductor Research Corporation (SRC)'s Nanoelectronics Research Initiative (NRI) via Midwest Institute for Nanoelectronics Discovery (MIND) and IBM for partial support of this research.

References

1. A. K. Geim and K.S. Novoselov, *Nature Materials,* **6,** 183-191, (2007)
2. A. A. Balandin, S. Ghosh, *et al.*, *Nano Letters,* **8**, 902-907, (2008).
3. S. Ghosh, I. Calizo, *et al.*, *Applied Physics Letters*, **92**, 151911(2008).
4. L. Wang and B. W. Li, *Physical Review Letters,* **101**, 267203, (2008).
5. B. W. Li, L. Wang, *et al.*, *Physical Review Letters,* **93**, 184301, (2004).
6. B. W. Li, L. Wang, *et al.*, *Applied Physics Letters,* **88**, 143501, (2006).
7. R. Murali, Y. X. Yang, *et al.*, *Applied Physics Letters,* **94**, 243114, (2009).
8. Z. Chen, W. Jang, *et al.*, *Applied Physics Letters,* **95**, 161910, (2009).
9. I. Calizo, S. Ghosh, *et al.*, *Solid State Communications,* **149**, 1132-1135, (2009).
10. I. Calizo, F. Miao, *et al.*, *Applied Physics Letters,* **91**, 151911, (2007).
11. N. Bonini, M. Lazzeri, *et al.*, *Physical Review Letters,* **99**, 176802, (2007).
12. M. Freitag, M. Steiner, *et al.*, *Nano Letters,* **9**, 1883-1888, (2009).
13. S. Subrina, D. Kotchetkov, A. A. Balandin, *IEEE Electron Device Letters,* **30**, 1281-1283, (2009).

14. P. Blake, E. W. Hill, *et al.*, *Applied Physics Letters,* **91**, 063124, (2007).
15. Q. Yu *et al., Applied Physics Letters,* **93**, 113103, (2008); H. Cao, *et al., Journal of Applied Physics,* in press, (2010), preprint at *arXiv:0901.1136* (2009)
16. X. S. Li, W. W. Cai, *et al.*, *Science,* **324**, 1312-1314, (2009); H. Cao, *et al.*, *arXiv:0910.4329* (2009)
17. J. N. Hu, X. L. Ruan, *et al.*, *Nano Letters,* **9**, 2730-2735, (2009).
18. Y. Xu, X. B. Chen, *et al.*, *Applied Physics Letters,* **95**, 233116, (2009).
19. Z. X. Guo, D. Zhang, *et al.*, *Applied Physics Letters,* **95**, 163103, (2009).
20. J. W. Jiang, J. S. Wang, *et al.*, *Physical Review B,* **79**, 205418, (2009).
21. J. N. Hu, *in preparation,* (2010).
22. N. Mingo, *Physical Review B,* **81**, 045408, (2010).
23. N. Yang, G. Zhang, *et al.*, *Applied Physics Letters,* **95**, 033107, (2009).
24. B. D. Kong, S. Paul, *et al.*, *Physical Review B,* **80**, 033406, (2009).
25. D. L. Nika, E. P. Pokatilov, *et al.*, *Physical Review B,* **79**, 155413, (2009).
26. D. W. Brenner, *Physical Review B,* **42**, 9458-9471, (1990).
27. W. G. Hoover, *Physical Review A,* **31**, 1695-1697, (1985).
28. S. Nose, *Journal of Chemical Physics,* **81**, 511-519, (1984).
29. L. Wang and B. W. Li, *Physical Review Letters,* **99**, 177208, (2007).